Role of Solvent-Host Interactions That Lead to Very Large Swelling of Hybrid Frameworks
C. Serre, *et al.*
Science **315**, 1828 (2007);
DOI: 10.1126/science.1137975

adsorbates. Specific paths for the ballistic transport of electrons through the molecules could be identified for C_{60} and PTCDA. They result from tunneling into the LUMO+1 electronic state followed by intramolecular transport and coupling to the bulk states of the underlying metal.

References and Notes

1. G. Timp *et al.*, *IEDM Tech. Digest*, 55 (1999).
2. A. Javey, J. Guo, Q. Wang, M. Lundstrom, H. Dai, *Nature* **424**, 654 (2003).
3. W. J. Kaiser, L. D. Bell, *Phys. Rev. Lett.* **60**, 1406 (1988).
4. L. D. Bell, W. J. Kaiser, *Phys. Rev. Lett.* **61**, 2368 (1988).
5. V. Narayanamurti, M. Kozhevnikov, *Phys. Rep.* **349**, 447 (2001).
6. P. L. de Andres, F. J. Garcia-Vidal, K. Reuter, F. Flores, *Prog. Surf. Sci.* **66**, 3 (2001).
7. W. H. Rippard, A. C. Perrella, R. A. Buhrman, *Appl. Phys. Lett.* **78**, 1601 (2001).
8. W. Li *et al.*, *J. Chem. Phys. B* **109**, 6252 (2005).
9. C. Troadec *et al.*, *Nanotechnology* **15**, 1818 (2004).
10. R. M. Feenstra, J. A. Stroscio, J. Tersoff, A. P. Fein, *Phys. Rev. Lett.* **58**, 1192 (1987).
11. R. J. Hamers, R. M. Tromp, J. E. Demuth, *Phys. Rev. Lett.* **56**, 1972 (1986).
12. B. C. Stipe, M. A. Rezaei, W. Ho, *Science* **280**, 1732 (1998).
13. C. Joachim, M. A. Ratner, *Proc. Natl. Acad. Sci. U.S.A.* **102**, 8801 (2005).
14. A. Nitzan, M. A. Ratner, *Science* **300**, 1384 (2003).
15. J. Park *et al.*, *Nature* **417**, 722 (2002).
16. H. W. Kroto, J. R. Heath, S. C. O'Brien, R. F. Curl, R. E. Smalley, *Nature* **318**, 162 (1985).
17. S. R. Forrest, *Chem. Rev.* **97**, 1793 (1997).
18. K. Glöckler *et al.*, *Surf. Sci.* **405**, 1 (1998).
19. W. Schottky, *Z. Phys.* **113**, 367 (1939).
20. F. Braun, *Pogg. Ann. Phys.* **153**, 556 (1874).
21. W. Mönch, *Electronic Properties of Semiconductor Interfaces* (Springer-Verlag, Berlin, ed. 43, 2004).
22. G. Binnig, H. Rohrer, Ch. Gerber, E. Weibel, *Appl. Phys. Lett.* **40**, 178 (1982).
23. G. Binnig, H. Rohrer, Ch. Gerber, E. Weibel, *Phys. Rev. Lett.* **50**, 120 (1983).
24. H. W. Fink, H. Schmid, H. J. Kreuzer, A. Wierzbicki, *Phys. Rev. Lett.* **67**, 1543 (1991).
25. C. Bobisch, A. Bannani, M. Matena, R. Möller, *Nanotechnology* **18**, 055606 (2007).
26. The experiments were performed at a sample temperature of 130 K with the use of a commercial instrument (Nanoprobe; Omicron, Taunusstein, Germany) that was modified for the requirements of the experiment. The instrument provides three STM units that can be operated independently. Atomic resolution [e.g., on Bi(111)] can be obtained with each tip. For our experiment, one of the additional STM tips was used to gently contact the metallic bismuth layer. To conduct BEEM, we chose tunneling currents between 10 and 50 pA as a compromise between the threshold for damaging the molecular layer and a reasonable signal-to-noise ratio for the current of ballistic electrons. At a tunneling current of 50 pA, the BEEM current typically amounted to 4 pA on the clean bismuth surface, 0.5 pA for most of the C_{60} molecules, and 3 pA for the PTCDA molecules.
27. H. Sirringhaus, E. Y. Lee, H. von Känel, *Phys. Rev. Lett.* **73**, 577 (1994).
28. C. R. Ast, H. Höchst, *Phys. Rev. B* **67**, 113102 (2003).
29. E. I. Altman, R. J. Colton, *Phys. Rev. B* **48**, 18244 (1993).
30. M. Prietsch, *Phys. Rep.* **253**, 163 (1995).
31. As discussed in several publications (*3*–*6*, *30*), for a constant distance between tip and sample, a good description is given by $I_{ballistic} \propto (E - E_B)^2$. However, in the experiment, the total tunneling current is kept constant and the distance increases as the bias is increased. Assuming a linear dependence between the tunneling current and the bias voltage, this can be corrected by dividing by the bias voltage (or electron energy).
32. R. Yamachika, M. Grobis, A. Wachowiak, M. F. Crommie, *Science* **304**, 281 (2004); published online 11 March 2004 (10.1126/science.1095069).
33. T. Ono, K. Hirose, *Phys. Rev. Lett.* **98**, 026804 (2007).
34. C. Rogero, J. I. Pascual, J. Gómez-Herrero, A. M. Baró, *J. Chem. Phys.* **116**, 832 (2002).
35. I. Chizhov, A. Kahn, G. Scoles, *J. Cryst. Growth* **208**, 449 (2000).
36. E. Umbach, M. Sokolowski, R. Fink, *Appl. Phys. A* **63**, 565 (1996).
37. R. Temirov, S. Soubatch, A. Luican, F. S. Tautz, *Nature* **444**, 350 (2006).
38. A. Hauschild *et al.*, *Phys. Rev. Lett.* **94**, 036106 (2005).
39. A. Hauschild *et al.*, *Phys. Rev. Lett.* **95**, 209602 (2005).

40. We thank H. Nienhaus and A. Lorke for fruitful discussions. Supported by the German Research Council within Sonderforschungsbereich 616, "Energy Dissipation at Surfaces."

Supporting Online Material

www.sciencemag.org/cgi/content/full/315/5820/1824/DC1
Figs. S1 to S5

11 December 2006; accepted 21 February 2007
10.1126/science.1138668

Role of Solvent-Host Interactions That Lead to Very Large Swelling of Hybrid Frameworks

C. Serre,[1]* C. Mellot-Draznieks,[1,2] S. Surblé,[1] N. Audebrand,[3] Y. Filinchuk,[4] G. Férey[1]

An unusually large expansion upon solvent adsorption occurs without apparent bond breaking in the network of a series of isoreticular chromium(III) or iron(III) diarboxylates labeled MIL-88A to D [dicarbox = fumarate (88A); terephthalate (1,4-BDC) (88B); 2,6-naphthalenedicarboxylate (2,6-NDC) (88C); and 4-4′-biphenyldicarboxylate (4-4′-BPDC) (88D)]. This reversible "breathing" motion was analyzed in terms of cell dimensions (extent of breathing), movements within the framework (mechanism of transformation), and the interactions between the guests and the skeleton. In situ techniques show that these flexible solids are highly selective absorbents and that this selectivity is strongly dependent on the nature of the organic linker.

Crystalline solids are normally quite rigid, but a reversible feature of some large-pore, hybrid, inorganic-organic crystalline solids is an unexpected swelling under external stimuli (such as pressure, temperature, light, or gas or solvent adsorption), sometimes with large magnitude (~5 Å) (*1*, *2*) in the variation of cell parameters. Such large volume variations suggest that these solids might have useful applications because of their selective adsorption, increased storage, and facile delivery (*3*, *4*).

The flexibility of hybrid organic-inorganic porous frameworks that enables these volume changes is governed by their host-guest interactions. Kitagawa (*3*, *5*) recently classified the different known behaviors of flexibility into six classes according to these interactions and the dimensions of the inorganic subnetwork, with the highest "breathing" amplitude so far being 40% (*2*). However, most of the studies reported have been limited to the structures of the frameworks at the initial and final stages of breathing but have not revealed the geometric changes and locations of the guests during the swelling that would provide insight into the mechanism of breathing. These necessary structural data are not always easy to obtain, because the swelling often breaks the crystals into powders, which are sometimes poorly crystallized.

We recently overcame these limitations by implementing a strategy based on a combination of targeted chemistry that controls the nature of the inorganic building block (*6*) and computer simulation (*7*). The structure of hybrid frameworks with giant cells [~380,000 $Å^3$ (*8*) and ~700,000 $Å^3$ (*9*)] can be determined for powdered samples by means of a direct space-computational strategy, by pushing the limits of conventional ab initio structure-determination methods of nonmolecular solids from synchrotron data. Moreover, when the crystal structure of a parent hybrid framework is known, lattice energy minimizations can be used to anticipate the series of related crystal structures experimentally obtained with linkers of greater size, with a simple ligand-replacement strategy in which the observed cell parameters of the series are used as target values. The simulations then provide the most likely atomic coordinates for the new framework (*10*), which may be directly used for further Rietveld refinements. The same combined approach was used successfully in the case study of the atypical iron(III) fumarate

[1]Institut Lavoisier, (UMR-CNRS 8180), Université de Versailles, 45 Avenue des Etats-Unis, 78035 Versailles Cedex, France. [2]Royal Institution of Great Britain, 21 Albemarle Street, London W1S 4BS, UK. [3]Sciences Chimiques de Rennes (UMR-CNRS 6226), Université de Rennes 1, Avenue du Général Leclerc, 35042 Rennes Cedex, France. [4]Swiss Norwegian Beamlines (SNBL) at the European Synchrotron Radiation Facility (ESRF), rue Jules Horowitz, 38043 Grenoble, France.

*To whom correspondence should be addressed. E-mail: serre@chimie.uvsq.fr

MIL-88A and allowed the elucidation of its structural transformations after adsorptions (*11*). In that system, a reversible expansion of ~85% was observed between the dehydrated and hydrated forms of MIL-88A, whereas other polar solvents (CH_3OH, C_2H_5OH, and C_4H_9OH) yielded intermediate variations in cell volume. Simulations provided an atomic-scale description of the structural changes involved in flexibility, yielding framework models for each host-guest system. The case study of MIL-88A illustrated how a flexible framework may adsorb a wide range of organic molecules or gases by simply adapting its framework structure. It also revealed to us that further exploration of this kind of framework was needed, together with a deeper understanding of the mechanisms at play.

We applied a similar strategy that combines observed cell parameters and lattice-energy minimizations for the analysis of the unusually large swelling without the apparent breaking of any chemical bond, in a series of isoreticular chromium(III) or iron(III) dicarboxylates formulated $[M_3^{III}O(H_2O)_2X(dicarbox)_3]$•guest (*10*) (M = Fe, Cr; X = F, Cl, acetate) and labeled MIL-88A to D (MIL standing for Materials of Institut Lavoisier) [dicarbox = fumarate (88A); terephthalate (1,4-BDC) (88B); 2,6-naphthalenedicarboxylate (2,6-NDC) (88C); and 4-4′-biphenyldicarboxylate (4-4′-BPDC) (88D)] (*10*). We characterized the breathing motion in three ways: (i) by the unit cell dimensions for the extent of swelling, (ii) by the movements within the framework for the mechanics of transformation, and (iii) from the guests and their interactions with the skeleton, which are the source of the movements. Below, we discuss the effect of swelling on the adsorption properties of different solvents.

The MIL-88 structure type is hexagonal (space group *P*-62*c* or $P6_3/mmc$) (*6*) and is built up from the connection of trimers of iron(III) or chromium(III) octahedra that share a μ_3-O oxygen with dicarboxylates (Fig. 1) in such a way that two types of cavities exist: tunnels along [001] and bipyramidal cages with trimers at the vertices. The height of the bipyramid corresponds to the *c* cell parameter, whereas *a* corresponds to the distance between two trimers in the equatorial plane. In a general way, the as-synthesized form (hereafter noted *as*) can accept solvents with a noticeable and continuous increase of the unit cell volume, one that maintains the same space group, to give the open form (hereafter noted as op) (figs. S1 to S4). Further desolvation through heating provides the desolvated form (hereafter noted as dry) while retaining the space group. During the reversible transformations, the Bragg peaks of the x-ray diffraction (XRD) powder patterns exhibit drastic but continuous displacements that are characteristic of a very large breathing effect and allow the refinement of the cell parameters of the different solids.

The data collection on the three powdered forms of each member of the series in its open form was performed at the European Synchrotron Radiation Facility (ESRF). Starting from the structures of the *as* forms, the application of our strategy (*8*) provided the starting atomic coordinates of the atoms of the hybrid framework for further Rietveld refinements (table S1 and figs. S5 to S7) (*12*).

The unit cell parameters (Fig. 2) increase almost linearly with the length of the linker, but, for each member, whereas the *c* parameter decreases by several angströms from the dry to the open form, the *a* axis drastically increases. The breathing phenomenon is anisotropic. The consequences for cell volume are spectacular, with a V_{op}/V_{dry} ratio (V_{op}, cell volume of the open form; V_{dry}, cell volume of the dried solid) that varies from 1.85 for the MIL-88A form to 3.3 for the MIL-88D form, which is considerably larger than the magnitude of breathing observed so far for hybrid solids (ratio ≤1.4). Such volume increases, between two- and threefold during insertion of guests, imply a reversible coordinated atomic movement of >10 Å, without any apparent bond breaking. For the sake of comparison, the similar ratio for lungs is only 1.4; furthermore, some polymers can expand to a comparable extent, but these materials are amorphous, whereas the MIL-88 solids stay crystalline, despite an anisotropic peak broadening, during all of the adsorption and desorption process. An interesting feature of the expansion is the lack of variation of the *a* parameter across the entire series of the dry form, which corresponds to the distance between trimers on each (001) plane. This *a* parameter remains almost constant within one estimated standard deviation, whatever the length of the linker. This indicates that, in the dry form, the building blocks are closely packed in the (001) plane, which excludes any further contraction. Thus, the interior of the bipyramid is not accessible to the guests, unlike the tunnels, which remain accessible even in the dry state. The initial stage of solvation will likely occur within the tunnels. Moreover, as already shown with MIL-88A (*11*), hydrophilic inorganic parts of constant thickness 2.9 Å alternate in these tunnels with hydrophobic organic groups whose thickness

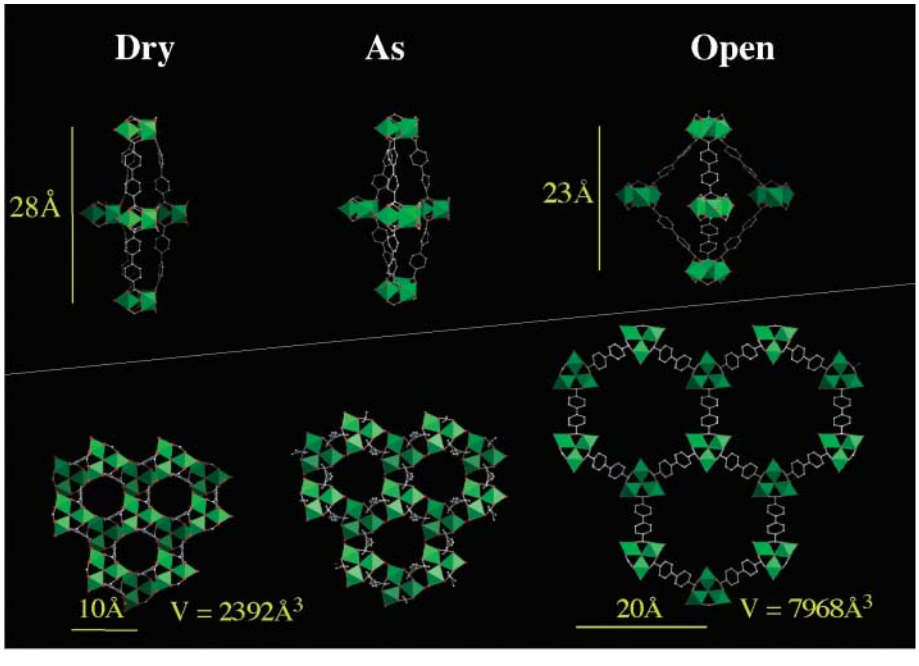

Fig. 1. (**Top**) Perspective view of the evolution of the bipyramidal cage of MIL-88D during the chemical (as → open) and thermal treatments (open → dry). (**Bottom**) Correlative evolution of the structure seen along [001]. Chromium octahedra, carbon, and oxygen atoms are green, red, and gray, respectively.

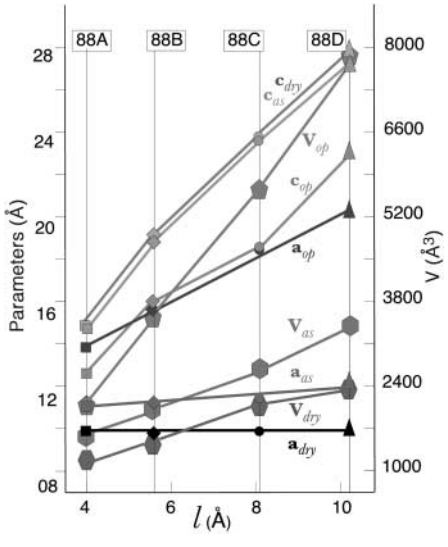

Fig. 2. Evolution of cell parameters and volumes of MIL-88 A through D in their different states (as synthesized, open, and dry) as a function of the length of the linker.

depends on the length of the linker (Fig. 1). This observation will help the explanation below of the different behaviors during resolvation.

What common characteristics of the frameworks allow such a reversible swelling? All of them exhibit, first, a continuous rotation of the trimers around [001] by a maximum of 30° during the transformation (Fig. 1). The O-O axis of the carboxylate functions acts as a "knee cap" (Fig. 3), around which the trimer and the phenyl rings can change their respective angular orientations, and allows rotations of the moieties that accommodate the constraints and minimize the lattice energy (see legend of Fig. 3 for details). This "mechanical" process, allowed by both the directivity of the covalent bonds of the linker and the lack of directivity of the metal-oxygen ionic bonds of the inorganic clusters, explains the softness of the transformations induced by host-guest interactions.

Once the swelling of the MIL-88 solids was rationally explained, we focused on how these interactions affect the selectivity of the adsorption process. The MIL-88 solids were soaked with various polar and nonpolar liquids. The breathing behavior is selective. Indeed, the pore opening strongly depends on the nature of the solvent, as shown in Fig. 4 by the XRD patterns of MIL-88C after immersion in various liquids. Depending on the chemical nature of the solvent, three degrees of pore opening are evidenced (Fig. 4 and Table 1): (i) small polar molecules (water and methanol) and apolar solvents (hexane and toluene) induced a small swelling magnitude, between 6 and 8% in volume; (ii) more hydrophobic but still polar liquids [butanol, dimethylcarbonate, dimethylformamide (DMF), and dimethylsulfoxide] generate a larger pore opening (15 to 60%), whereas (iii) pyridine and diethylformamide (DEF) completely open the structure, with a resulting huge increase in cell volume of about 165 to 170% (Table 1).

The reason for such dissimilarities in the magnitude of opening must be found in the characteristics of the tunnels and from the nature of the guest and its associated interactions. Indeed, we already noted above that hydrophilic inorganic parts of constant thickness 2.9 Å (free aperture 3.7 Å for MIL-88C) alternate in the tunnels with hydrophobic organic parts (free aperture 3.2 Å), the thickness of which depends on the length of the linker. Thus, several types of interactions are possible in MIL-88C: (i) Similar to those with MIL-88A (*10*, *11*), small polar liquids may interact with the inorganic trimers of metal(III) octahedra (coordination of the metal, hydrogen bond interactions). (ii) Weak interactions are expected with the organic linker, such as van der Waals, π-π, and CH-π interactions. Nonpolar liquids interact only with the linker, and the presence of some coordinated terminal water molecules in the trimers does not favor their adsorption into the framework. More hydrophobic polar liquids interact preferentially with the organic parts of the tunnels [as proved by the structure of MIL-88C filled by pyridine (fig. S8)] and increase the number of CH-π interactions, which explains why butanol is more adsorbed than methanol or ethanol. For the same reason, DMF and DEF generate a larger pore opening in MIL-88C. More surprising, however, is the very large difference in pore opening magnitude observed for MIL-88C when 2,6-dimethyl pyridine (lutidine) (V_{op}/V_{dry} = 107 to 108%) is used instead of pyridine (V_{op}/V_{dry} = 265 to 270%). Pyridine is well known for its ability to interact strongly with polar moieties or to coordinate the metals and to interact with aromatic rings from the naphthalene linker through π-π interactions; in the case of the 2,6-dimethyl pyridine, the steric hindrance of the methyl groups considerably weakens such interactions and thus drastically decreases its adsorption by the porous framework. These features illustrate the competition during the adsorption process between the inorganic and the organic parts of the tunnel for attracting the guest molecules depending on their nature and steric hindrance.

However, MIL-88C presents differences from the other members of the MIL-88 series that relate to the orientation of the phenyl rings in MIL-88C, which are orthogonal to those

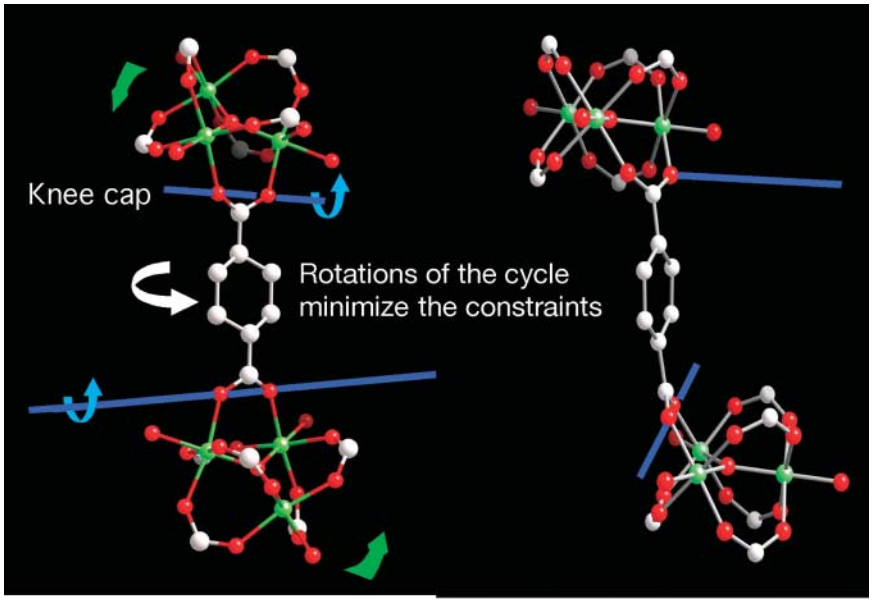

Fig. 3. Part of the structure of the cage in MIL-88B, which corresponds to one edge of the trigonal bipyramid. It illustrates the framework displacements during breathing, which occur around the knee cap O-O axis [blue line and sense of rotation (blue arrow)] of the carboxylates. This allows the rotation around this axis of the whole trimeric units (green arrows). The free rotations of the phenyl ring and of the trimers around the OOC-COO axis only relax the constraints and minimize the lattice energy during the transformation. Chromium, carbon, and oxygen atoms are green, red, and white, respectively.

Fig. 4. Evolution of the XRD patterns for MIL-88C in various solvents at room temperature (arbitrary units).

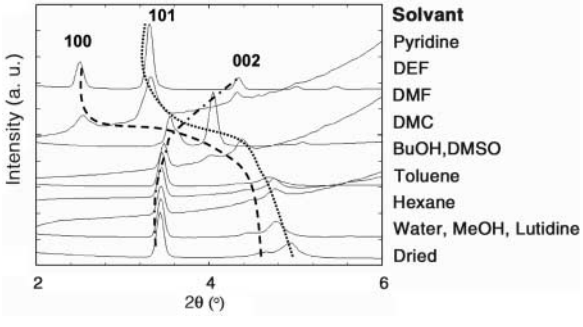

Table 1. Cell volumes and the breathing amplitudes for MIL-88C at its largest expansion relative to the dry form (2120 Å^3).

Solvent	Cell volume	
	Initial (Å^3)	V_{op}/V_{dry} (%)
Pyridine	5695	270
DEF	5600	265
DMF	3415	160
DMC	2775	130
BuOH, DMSO	2435	115
Toluene	2295	108
Hexane	2285	108
Water, MeOH, lutidine	2270	107

of MIL-88B and MIL-88D (fig. S9). Unlike MIL-88C, the plane of the rings in the other members points toward the interior of the tunnel and leaves less room for adsorption, especially for MIL-88D. When starting from the dried form, the pore opening remains rather weak (<20%) when the solid is dispersed at room temperature in a liquid, despite the importance of the organic linker (fig. S10). Alternatively, the use of the as-synthesized form of MIL-88D leads to an almost MIL-88B–like adsorption behavior (figs. S11 and S12); with adsorption of different liquids, the magnitude of pore opening depends, once more, on the nature of the guest. Besides the specific interactions between solvent molecules and the framework, a geometrical threshold exists for an adsorption in the tunnels. Moreover, this threshold is thermally activated, because at 150°C, dispersion of MIL-88D in pyridine leads to its total opening (fig. S13). The same behavior is observed for MIL-88C in its dried state. Dispersed in DMF at room temperature, it exhibited a 60% pore opening, whereas the same experiment performed at 150°C showed a total opening (170%) (fig. S14). However, thermodynamically, if there is a thermal effect related to the pore opening of the framework, it is masked by that of solvation, which occurs simultaneously.

We can briefly discuss the kinetics of adsorption. From our experiments, it seems that the kinetics of breathing is distinctive for each MIL-88–solvent association. For example, MIL-88A and MIL-88B breathe within a few seconds in the presence of ethanol, whereas it takes several days for MIL-88B to open its pores completely in the presence of water or nitrobenzene (figs. S15 and S16). Similarly, MIL-88C opens rapidly with pyridine (<1 min) but slowly with DEF (hours).

Finally, it is not known whether there is a phase transition when a solvent is adsorbed. The nets are topologically invariant and are not reconstructed between the different forms. In this sense, if there is a transition, it might be only a displacement, but even in this case, most of the structural transitions are associated with a change in symmetry and, therefore, in the XRD patterns. Here, the space group remains the same (*P*-62*c* or $P6_3/mmc$), and the patterns show a continuous evolution (figs. S17 to S20). Thus, this breathing phenomenon is reversible for each solid and without any apparent loss of crystallinity, even if anisotropic peak broadening is observed with drying for the (hk0) Bragg reflections while (001) peaks retain their initial width. However, the anisotropy disappears with wetting, and both (hk0) and (001) reflections recover the same peak width, which also rules out the appearance of an impurity or a structural change during the breathing phenomenon. At first glance, the peak broadening with drying could be due to some disorder (residual molecules of solvent) in the (*ab*) plane.

The cyclability of the breathing phenomenon has not been addressed so far. However, we have observed by XRD that the pore opening still occurs with no apparent loss of crystallinity after a few desolvation-solvation cycles (fig. S17 to S20). Further investigations will be needed in order to understand both the energetics and the cyclability of this breathing phenomenon.

References and Notes

1. K. Barthelet, J. Marrot, D. Riou, G. Férey, *Angew. Chem. Int. Ed.* **41**, 281 (2002).
2. C. Serre *et al.*, *J. Am. Chem. Soc.* **124**, 13519 (2002).
3. S. Kitagawa, K. Uemura, *Chem. Soc. Rev.* **34**, 109 (2005).
4. A. J. Fletcher, K. Thomas, M. Rosseinsky, *J. Solid State Chem.* **178**, 2491 (2005).
5. K. Uemura, R. Matsuda, S. Kitagawa, *J. Solid State Chem.* **178**, 2420 (2005).
6. C. Serre, F. Millange, S. Surblé, G. Férey, *Angew. Chem. Int. Ed.* **43**, 6285 (2004).
7. C. Mellot-Draznieks, J. Dutour, G. Férey, *Angew. Chem. Int. Ed.* **43**, 6290 (2004).
8. G. Férey *et al.*, *Angew. Chem. Int. Ed.* **43**, 6296 (2004).
9. G. Férey *et al.*, *Science* **309**, 2040 (2005).
10. S. Surblé, C. Serre, C. Mellot-Draznieks, F. Millange, G. Férey, *Chem. Commun.* **2006**, 284 (2006).
11. C. Mellot-Draznieks *et al.*, *J. Am. Chem. Soc.* **127**, 16273 (2005).
12. Supplementary data and figures are available on *Science* Online.

13. We are indebted to the ESRF in Grenoble for providing beamtime and for the help of the staff during and after the experiments. F. Millange and G. Marsolier are also acknowledged for their help in collecting XRD patterns. CNRS is acknowledged for financial support. Coordinates of MIL-88A to D deduced from computer simulation (dry, open forms) as well as the experimental structures of the open forms of MIL-88A to D (with solvents) have been deposited with ICSD data bank, deposition numbers CSD 417746, 417747, 417748, 417749, 417750, 417751, 417752, 417753, 417756, 417757, 417758, and 417759.

Supporting Online Material

www.sciencemag.org/cgi/content/full/315/5820/1828/DC1
Materials and Methods
Figs. S1 to S20
Table S1
References

27 November 2006; accepted 21 February 2007
10.1126/science.1137975

Plastic Deformation Recovery in Freestanding Nanocrystalline Aluminum and Gold Thin Films

Jagannathan Rajagopalan, Jong H. Han, M. Taher A. Saif*

In nanocrystalline metals, lack of intragranular dislocation sources leads to plastic deformation mechanisms that substantially differ from those in coarse-grained metals. However, irrespective of grain size, plastic deformation is considered irrecoverable. We show experimentally that plastically deformed nanocrystalline aluminum and gold films with grain sizes of 65 nanometers and 50 nanometers, respectively, recovered a substantial fraction (50 to 100%) of plastic strain after unloading. This recovery was time dependent and was expedited at higher temperatures. Furthermore, the stress-strain characteristics during the next loading remained almost unchanged when strain recovery was complete. These observations in two dissimilar face-centered cubic metals suggest that strain recovery might be characteristic of other metals with similar grain sizes and crystalline packing.

In coarse-grained metals, dislocation-mediated processes govern plastic deformation, with the dislocations generated by intragranular sources. Dislocations propagating in intersecting slip planes can interact with each other and, in the process, form new dislocations that are immobile. These immobile dislocations obstruct the passage of other slip dislocations through these planes and harden the crystal, a phenomenon commonly referred to as work hardening (*1*).

Nanocrystalline metals, where the grain size is typically less than 100 nm, are expected to behave differently because the grain size is smaller than the characteristic length scales associated with nucleation and propagation of dislocations (*2*–*4*). Experiments (*5*, *6*) indicate that intragranular dislocation sources like the Frank-Read source cease to operate in nanocrystalline metals, although in situ transmission electron microscopy (TEM) observations of tensile deformation have shown dislocation activity, especially near crack tips (*7*). The lack of dislocation sources results in high strength and reduced plasticity in these materials (*8*, *9*), although recent experiments (*10*) indicated that stress-assisted grain growth during deformation can lead to enhanced ductility. Atomistic simulations suggest that dislocations nucleated at grain boundaries (GBs) carry out plastic deformation in the nanocrystalline regime; once nucleated, these dislocations travel across the grains and are eventually absorbed in the opposite GB (*11*–*13*). Atomistic simulations and experiments also suggest that, at very small grain sizes (~10 nm), GB sliding and migration become the dominant deformation mechanisms and cause a reduction in strength (*14*–*17*).

Although the behavior of nanocrystalline metals during deformation has been investigated, their postdeformation behavior has received little

Department of Mechanical Science and Engineering, University of Illinois at Urbana-Champaign, Urbana, IL 61801, USA.

*To whom correspondence should be addressed. E-mail: saif@uiuc.edu